UPPSALA
UNIVERSITET

ELEKTRO-MFE 22003
Master's Thesis 30 credits
September 2021

Design Optimization of Savonius Wind Turbine using CFD Simulations

Vatsalkumar Arvindbhai Manavar

Masterprogram i förnybar elgenerering

Master Programme in Renewable Electricity Production

UPPSALA
UNIVERSITET

Faculty of Science and Technology

Visiting address:
Ångströmlaboratoriet
Lägerhyddsvägen 1
House 4, Level 0

Postal address:
Box 536
751 21 Uppsala

Telephone:
+46 (0)18 – 471 30 03

Telefax:
+46 (0)18 – 471 30 00

Web page:
http://www.teknik.uu.se/student-en/

Abstract

Design Optimization of Savonius Wind Turbine using CFD Simulations

Vatsalkumar Manavar

This thesis is based on simulation of the Savonius wind turbine. The Savonius turbine is a simple vertical axis device, which has half cylindrical blades attached to the main shaft in opposite to each other which creates the drag force from incoming wind and generates mechanical torque which drives the generator for electricitygeneration.

The main aim is to investigate the best design of two bladed verticalaxis Savonius wind turbine. Study investigates the aerodynamics and design optimization of wind turbine. For an automation purpose, CAESES software is used to design different blade profiles and ANSYSMultiphysics software is used to simulate the different geometries inconnection with CAESES software.

A validation study is performed, and the generated data are compared with previous study to validate the simulation model. The studied parameters are, blade arc angle, distance between blades, and overlap ratio of blades. The findings show that the most efficient profile has a blade arc angle of 110 degree. The optimal distance between blades was found to be 3.1 cm with an overlap ratio of 0.25.

Keywords: Savonius wind turbine, Computational fluid dynamics,Vertical axis wind turbine, Overlap ratio, Distance between blades, Power coefficient

Supervisor: Anders Goude
Subject reader: Hans Bernhoff
Examiner: Irina Temiz
ELEKTRO-MFE 22003
Printed by: Uppsala University

Popular scientific summary

Global energy consumption is increasing gradually, and at the same time, the usage of fossil fuels is also increasing. To control global emissions, it is necessary to switch to renewable energies. Amongst all renewable resources, majority of renewable energy can be generated by means of solar power, wind power, hydropower, biomass and geothermal resources. According to IRENA's latest data, global installed wind generation capacity has been increased by a factor of 75 in the past two decades.

Wind turbines are classified into two types, Horizontal axis wind turbines and vertical axis wind turbines. The Savonius turbine is a simple vertical axis device that has half-cylindrical blades attached to the main shaft opposite to each other. Low noise and easy design make this turbine type unique for small and remote applications. Irrespective of wind direction, this drag based turbine profile has been becoming a mutual interest of researchers.

The aim of this project is to investigate the efficiency of the Savonius type vertical axis wind turbine by investigating the aerodynamic performance. The study includes the aerodynamic efficiency and design of turbine profile. Design modifications play an important role in the efficiency of the turbine. Two design modifications have been investigated in this work, distance between two blades and Overlap ratio of blades. To compare the different turbine geometries, power coefficient and torque coefficients were used to compare the findings with the previous study. The analysis was carried out numerically in Ansys Fluent using 2D simulations. The partial differential equations are used to characterize the flow properties, including turbulence effects, solved using Reynolds Average Navier stokes in combination with the k-ω SST model.

Experimental data were compared to simulated experimental values of the ModBach profile for validation. ModBach profile is developed by the Roy and Saha. Which is further studied by many researchers. The most efficient profile has a blade arc angle of 110 degrees. The optimal distance between blades was found to be 3.1 cm with an overlap ratio of 0.25.

Acknowledgement

I want to thank my supervisor **Anders Goude**, subject reader **Hans Bernhoff** and examiner **Irina Temiz** for allowing me to work on this research topic within the department of Electrical Engineering, Uppsala University.

I want to thank my supervisor for constant guidance and support in my thesis work. He has helped me for setting up my simulation setup. Also, I would like to thank my colleague Sascha Thomas for his guidance in simulation setup and his company in working on the same project. I would also like to thank my study counsellor **Juan de Santiago** for supporting and helping throughout my masters studies at Uppsala University.

Last but not least, I would also like to thank my family especially my **father (Arvindbhai)**, **mother (Mintuben)**, **sister (Ami)** and **Friends** for being there for me through my good and bad times.

Table of Contents

Abbreviations 7

Nomenclature 7

List of Tables 8

List of Figures 8

1. Introduction 9

1.1 Wind Energy 9

1.2 Background 10

1.3 Aim 10

1.4 Research Questions 10

1.5 Limitations and Assumptions 11

2. Theory 12

2.1 Fundamentals of Vertical axis wind turbine 12

2.1.1 Different types of VAWT 12

2.2 Savonius Wind Turbine 13

2.2.1 Power Characteristics 13

2.2.2 Betz energy extraction limit 14

2.2.3 Different Savonius Blade Profiles 16

3. Geometry Selection 17

4. Design and Simulation Methodology 18

4.1 Software 18

4.1.1 CAESES 18

4.1.2 Ansys 19

4.2 Simulation Setup 25

4.2.1 Simulation Domain Validation 28

5. Results 29

5.1 Validation 29

5.2 Distance Between Blades 30

5.3 Overlap Ratio 31

6. Discussion 34

7. Conclusion 36
8. Appendix 39
8.1 Studied parameters in this study 39
8.2 Dimensions of important geometries from Study 1&2 39
8.3 Selection of Viscous Model constants which are used in the simulations 40

Abbreviations

2-D	Two Dimensional
3-D	Three Dimensional
CAD	Computer Aided Design
CFD	Computational Fluid Dynamics
CFL	Courant Friedrichs Lewy
DP	Design Point
HAWT	Horizontal Axis Wind Turbine
OR	Overlap Ratio
RANS	Reynolds Averaged Navier Stokes
SSWT	Small-Scale Wind Turbine
SST	Shear Stress Transport
TSR	Tip Speed Ratio
VAWT	Vertical Axis Wind Turbine

Nomenclature

ρ	kg/m^3	Air density
λ	-	Tip speed ratio
ω	rad/sec	Angular velocity
A	m^2	Turbine cross-sectional area
A_∞	m^2	Inlet cross-section area of stream tube
D	m	Turbine diameter
d	m	Blade cup diameter
P	W	Power absorbed by the turbine
R_e	-	Reynolds number
u_T	cm/s	Friction velocity
V	m/s	Wind velocity
V_e	m/s	Wind velocity behind the turbine
V_d	m/s	Wind velocity at the disc of turbine

List of Tables

Table 1: CP, Max and $PMax$ data for different geometries developed by [4]. 17
Table 2: Selected meshing size of refinements and rotor face 28
Table 3: Selected best geometries from Distance between blade analysis to investigate OR 31
Table 4: Dimensions of Selected Geometries to Investigate the Overlap Ratio 31
Table 5: Study of Overlap Ratio parameter on selected three geometries 32

List of Figures

Figure 1: Trend of global new wind energy installations 9
Figure 2: Types of VAWT rotor (a)Savonius (b)Darrieus (c)H-Darrieus (d)Helix shape [7] 12
Figure 3: C_p curve of different designs averaged to tip speed ratio [10] 14
Figure 4: Illustration shows the control volume used for momentum conservation [12]. 15
Figure 5: Traditional Savonius Rotor [11]. 16
Figure 6: Various blade profiles generated by Roy and Saha [13] 16
Figure 7: Selected geometries with blade arc angle of 110°, 130° and 150° (left to right) 17
Figure 8 Top view representation of Blade arc angle 18
Figure 9 Top view representation of Distance between blades 19
Figure 10: Top view of blade profile with a parameters of Overlap Ratio 19
Figure 11: Meshing used for the simulation 21
Figure 12: Plot of $y+$ plus data values of blade 1 23
Figure 13: CFL value correction during the ongoing simulation 24
Figure 14: Project Schematic in ANSYS Workbench 25
Figure 15: Different phases of Fluent setup 26
Figure 16: Automated Simulation Cycle 27
Figure 17: Different geometries in Parameter Set 27
Figure 18: Dimension of simulation domain in terms of turbine diameter [4] 28
Figure 19: Cq and Cp results for different blade angles[2] 29
Figure 20: Cq and Cp results of selected blade angles 29
Figure 21: Cp result of 18 geometries by varying the distance between blades(@ TSR=1) 30
Figure 22: Selected geometries to investigate the overlap ratio. Left to right, first geometry is 110° with 3.1cm, second 130° with 3.5cm, and last 150° with 2.5cm distance between blades .. 31
Figure 23: Overlap Distance study of three profiles with different overlap ratios (@TSR=1) 32
Figure 24 Top view visual representation of Savonius rotor profile 39
Figure 25 Selected blade profiles 110°,130°,150° (left to right) 39
Figure 26 Selection of Viscous Model constants 40

1. Introduction

1.1 Wind Energy

In the last few decades, the adoption of renewable energy sources has increased rapidly. Especially wind and solar energy are becoming primary renewable sources due to advancements in technology. However, wind energy has become a mature technology in renewables. According to GWEC historical data, the year 2020 is showing 93 GW of new wind power installation compared to 2019, which makes total installed wind power to 743 GW [1]. The representation of new offshore and onshore wind power installation is shown in figure 1.

Figure 1:Trend of global new wind energy installations[1]

In the past few years, research and new advancement in wind turbine technology has increased for onshore and offshore wind turbine technology. Mainly wind turbines are classified into two types, horizontal axis wind turbine (HAWT) and vertical axis wind turbine (VAWT). Out of those two, HAWTs are more efficient due to its mature technology. VAWTs are mainly classified into two types, Savonius type and Darrius wind turbine. In the past decade, many studies have been done on various VAWT. Savonius wind turbine has proven its capabilities in turbulent flow conditions. Due to simple and robust construction, it's primarily installed in remote areas where the grid connection is not available. Till now various savonius design have been developed and investigated. This technology is mainly focused on small applications, so it won't be able to give a major contribution to the total installed power of the world. A brief discussion on Savonius and other VAWTs is provided in the theory section.

The main advantage of VAWT is that irrespective of horizontal wind direction, it can absorb the wind, so it doesn't require a yaw control mechanism. Another key advantage of VAWT is, it requires less starting torque due to its small design. Additionally, VAWTs are robust and simple in design. Significant components of VAWT are placed on the ground, which makes turbine maintenance easy [2]. While in large scale HAWT, maintenance and commissioning is complex compared to small scale VAWTs. These days small off-grid application prefers to use hybrid wind and solar energy sources [3]. In such an application, VAWT could be used for electricity generation.

Recent advancements and developments in wind power technology have led to many types of vertical and horizontal type wind turbines. The current market provides wind turbines that can generate a few kW up to 10 MW rated power. In this extensive range of generation capacity, HAWTs have market dominance due to their efficiency and technology maturity. Whereas

VAWTs are also quite famous for small applications. In this thesis, we will discuss more on types of VAWT in the theory section.

1.2 Background

Various studies on VAWT have been done so far. Some of them are focused on the Savonius rotor's aerodynamics, and others are concentrated on design. Modified bach (ModBach) type profile developed by Roy and Saha has given good efficiency [4], which is modified and studied further by Lundberg, Manousidou, Solhed and Sundberg [4]. According to [4]–[6], the Modified Bach type has proven its efficiency compared to the previous classical bach type blade profile. In addition, findings show that increasing blade arc angle gives a higher power coefficient when it's compared to the conventional semi-circular and semi-elliptic blade profiles (figure 6). In the present investigation, a design optimization study has been carried out for the ModBach profile developed by [5]. All investigations are done by using computational fluid dynamic (CFD) simulations.

By observing the data of the Savonius turbine's different studies, it can be concluded that the shape of the savonius rotor plays an important role. It is perceived that the number of blades and blade arc angles are studied extensively. It is vital to study further on the distance between blades, overlap ratio and other design parameters, which is not investigated yet.

1.3 Aim

This thesis is based on simulations of the aerodynamics of wind turbines. This thesis aims to optimize the design of the Savonius turbine and increase the power coefficient of the Savonius wind turbine. Much research has been done on Savonius wind turbines, and there are several designs published so far. This study is a continuation of previous work titled "*Two-dimensional Study of Blade Profiles for a Savonius Wind Turbine*"[5]. In this thesis, study includes the best overlap ratio and optimum distance between blades by considering the power coefficient. The study is performed on three geometries (110°, 130°, and 150° blade arc angles) with six different distances between blades for each geometry, which sums up 18 geometries. After investigating those geometries, for each blade angle, one best design has been investigated further to find the best overlap ratio.

1.4 Research Questions

From a design and efficiency optimization point of view, there are three research problems created to investigate further in connection with previous studies.

1. Optimum distance between blades of Savonius wind turbine
2. Best overlap ratio of blades
3. Consideration of varied radius in the calculation of power coefficients

1.5 Limitations and Assumptions

In this study, due to limited time frame and computational power, all the simulations are carried out on personal PC with the limited computational power. In addition to the that, simulation domain has some flow limitations which is discussed in 4.1.2.4. In addition, All the simulation are performed at constant 8 m/s wind velocity with zero shear. Boundary conditions are introduced into the simulation domain to analyze specific parameters related to Savonius Rotor. Couple of constants are also introduced into the turbulence model (4.1.2.3).

2. Theory

In this section the fundamental theory of vertical axis wind turbine, fluid mechanics, computational fluid dynamics are discussed in brief. Different blade geometries and essential concepts of simulation setup are also presented along with turbine theory.

2.1 Fundamentals of Vertical axis wind turbine

From a design point of view, vertical axis wind turbines are different compared to HAWT. All turbines with the wind perpendicular to the axis of rotation are generally considered VAWT, independent of the actual direction of the axis. Savonius type VAWT are drag based turbines, and the drag mechanism makes them different from HAWT. The turbine patented by Finnish engineer, Sigurd Johannes Savonius is the most famous drag based VAWT. After his name, the name of the turbine profile is known as Savonius VAWT [4]. Current studies show higher power coefficient potential with different geometries. All new experimental geometries have their own advantage over other designs. In this report, we will discuss the Modified Bach Savonius Wind Turbine, as the design did exist before, and it is mainly studied in [3].

2.1.1 Different types of VAWT

Mainly VAWTs are divided into two major types:

1. Savonius- drag driven
2. Darrius- lift driven

From design point of view, Savonius turbines are simple compared to Darrius turbines. Savonius turbines contains two semi-cylindrical cups attached to the vertical shaft in such a way that it can create drag forces and rotate around the vertical axis. Figure 2(a) shows the design of the Savonius wind turbine, followed by the Darrius-rotor figure 2(b).

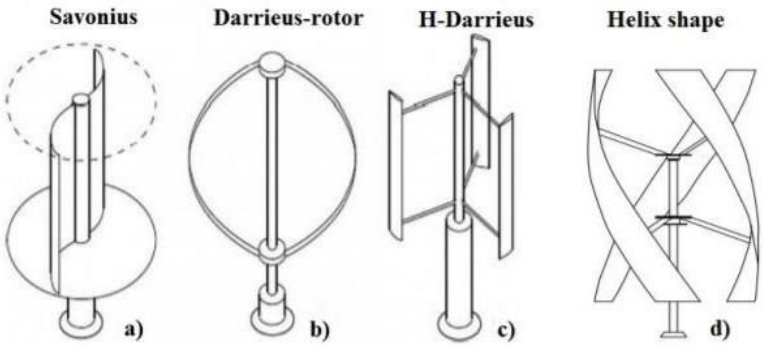

Figure 2: Types of VAWT rotor (a)Savonius (b)Darrieus (c)H-Darrieus (d)Helix shape [7]

Figure 2(b-d) shows the different types of Darrius turbine profiles. Figure 2(b) is developed to reduce the centrifugal loads, 2(c) is to get a larger cross-sectional area, which makes it easier to manufacture and allows high tower height, and 2(d) is to reduce the torque and thrust oscillations. According to previous research, the efficiency of the Savonius Turbine is lesser than the Darrius Turbine. Savonius turbines are used where the cost and reliability are considered as the main

parameter [6]. Additionally, Savonius turbines are preferred mainly for small sizes, as power scales as R^2 but mass scales as R^3.

2.2 Savonius Wind Turbine

Johann Ernst Bessler made the first attempt to build such a wind turbine in Furstenberg, Germany, in 1745 [8]. Savonius turbine is a simple vertical axis device. Depending on total number of blades, it has half-cylindrical blades attached to the main shaft opposite to each other (for two bladed), which creates the drag force from incoming wind and generates mechanical torque, which drives the generator for electricity generation.

2.2.1 Power Characteristics

Total power available from wind for electricity generation can be calculated from the following equation (2.1),

$$P = \frac{1}{2} V^2 \rho A V \quad (2.1)$$

Here, ρ is air density (kg/m^3)

V is the wind speed (m/s)

A is the cross-sectional area of the turbine.

Equation (2.1) shows the multiplication of kinetic energy and mass flow rate, which gives the total power available (in watts) from the wind [9]. Usually, the power coefficient C_p, characterizes the performance of the rotor. It shows the efficiency of the turbine. According to the Betz limit, theoretically maximum possible efficiency is 59.3% which is shown as rotor power limit in figure 3 [10]. Betz limit is discussed briefly in section 2.2.2. Mathematically C_p can be written as follows,

$$C_p = \frac{Q\mathrm{n}}{\frac{1}{2}\rho V^3 A} \quad (2.2)$$

Equation (2.2) is valid for three-dimensional calculations. Since the investigation is done in two-dimensional mode, the area of the turbine can be written as A=2R. Therefore, the modified equation can be written as follows.

$$C_p = \frac{Q\mathrm{n}}{\rho V^3 R} \quad (2.3)$$

Another important parameter is tip speed ratio (TSR) which is helpful to study the turbine performance at different rotational velocities. The tip speed ratio is defined by λ, and mathematically it can be written as the ratio between the tip speed of the blade to the inlet wind velocity.

$$\lambda = \frac{\mathrm{n}R}{V} \quad (2.4)$$

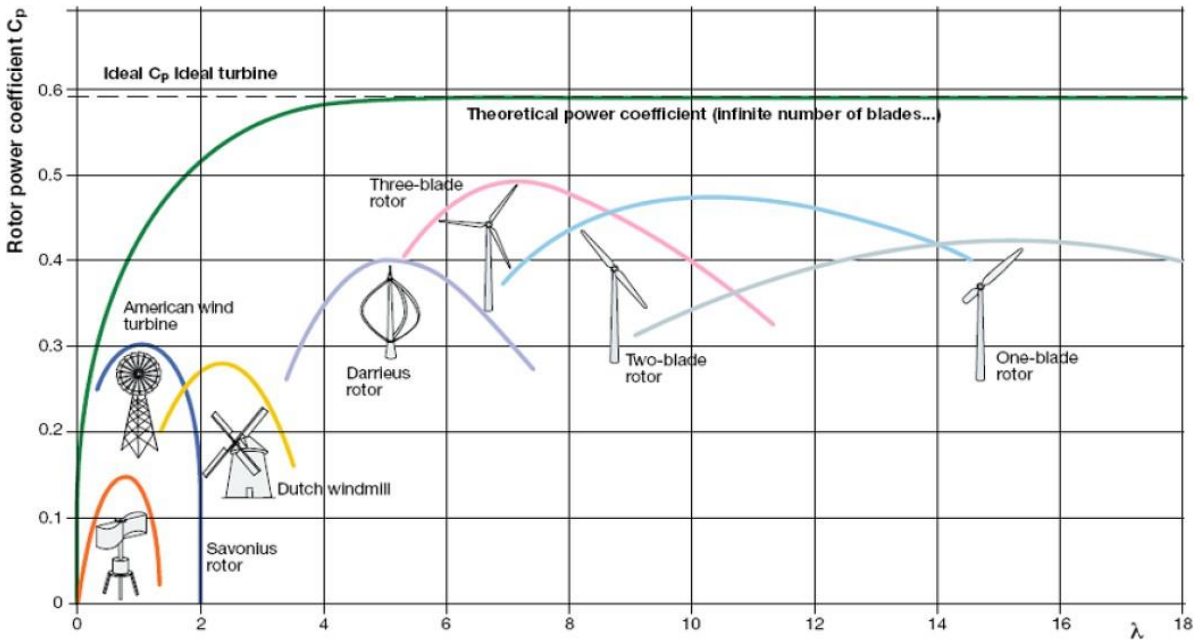

Figure 3: C_p curve of different designs averaged to tip speed ratio [10]

Usually, the turbine power curve is plotted against the TSR. At different TSR turbine gives different efficiency. In this thesis, except for the validation part, all the simulations are performed at TSR 1.

2.2.2 Betz energy extraction limit

The Betz theory determines the maximum power generation from the turbine rotor. This model is entirely based on linear momentum theory developed over 100 years ago to predict ship propellers performance [10]. This law is derived from the conservation of energy, momentum and mass principle. There are some limitations and assumptions like incoming wind speed, passing through turbine swept area is considered as uniform. It considers an infinite number of blades, no hub, uniform thrust over the rotor area and the static pressure far upstream and downstream should be equal to undistributed ambient static pressure. It is essential to have a change in wind speed from upstream to downstream to extract the energy from the turbine. According to the implication from the Betz equation, no change ($V_\infty = V_e$ figure 4) in wind speed leads to zero energy extraction from the wind.

If we consider the wind speed passing through turbine disk as V_d, with two different position values V_∞ (upstream) and V_e (downstream), Anders Goude's work shows the schematic illustration and derivation of Betz limit [11]. Mathematically it can be expressed as,

$$V_e < V_\infty \quad (2.5)$$

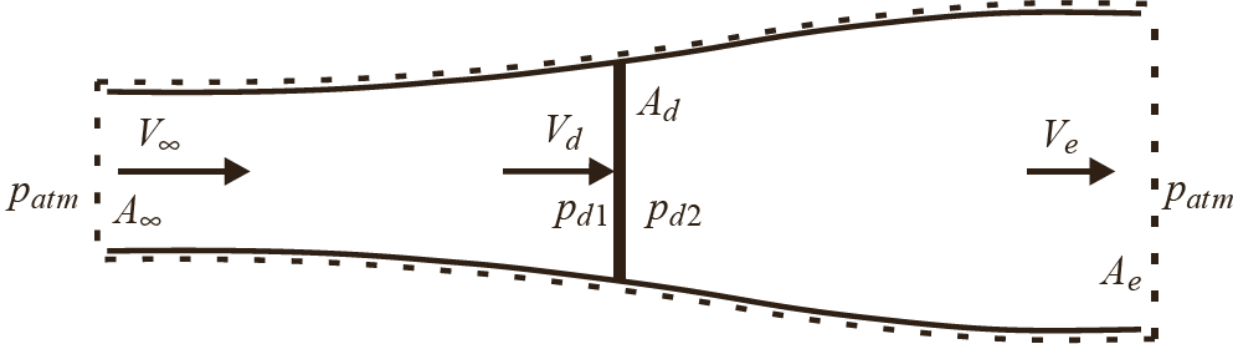

Figure 4: Illustration shows the control volume used for momentum conservation [12].

If we apply the Bernoulli equation in the above-mentioned flow tube of the turbine,

$$P_{atm} + \frac{1}{2}\rho V_\infty^2 = P_{d1} + \frac{1}{2}\rho V_d^2 \quad (2.6)$$

$$P_{d2} + \frac{1}{2}\rho V_d^2 = P_{atm} + \frac{1}{2}\rho V_e^2 \quad (2.7)$$

Equation (2.6) is for upstream, whereas equation (2.7) is written for downstream of the turbine. When we combine both with continuity, we can write as follows.

$$V_\infty A_\infty = V_d A_d = V_e A_e \quad (2.8)$$

Equation (2.5) shows there is a drop in wind speed. This happens due to momentum conservation inside the tube control volume. In figure 4, momentum conservation for dashed line (volume of wind) can be written as,

$$A_d(P_{d2} - P_{d1}) = \rho A_e V_e^2 - \rho A_\infty V_\infty^2 \quad (2.9)$$

As discussed at the beginning of this section that Betz theory has some assumptions. By considering no losses, the power absorbed by a wind turbine can be written as the difference between the incoming and outgoing power in the air,

$$P = \frac{1}{2}\rho A_\infty V_\infty^3 - \frac{1}{2}\rho A_e V_e^3 \quad (2.10)$$

Therefore, the air stream cross-section will increase from upstream of the turbine to downstream of the turbine, which leads to the pressure difference and wind speed drop. The derivation of Betzlaw shows that the downstream velocity should be one-third of upstream velocity for optimal conditions. Optimal power is given by,

$$P = \frac{16}{27} \cdot \frac{1}{2}\rho A_d V_\infty^3 \quad (2.11)$$

In equation (2.11), 16/27 shows the traditional Betz limit, limiting the power coefficient to 59.3%. Figure 3 shows this limit as a theoretical power coefficient limit.

2.2.3 Different Savonius Blade Profiles

In this section, we will discuss about the different blade profiles and the motivation behind those profiles. Figure 5 shows the traditional Savonius rotor, which represents all dimensions of a two-bladed Savonius rotor.

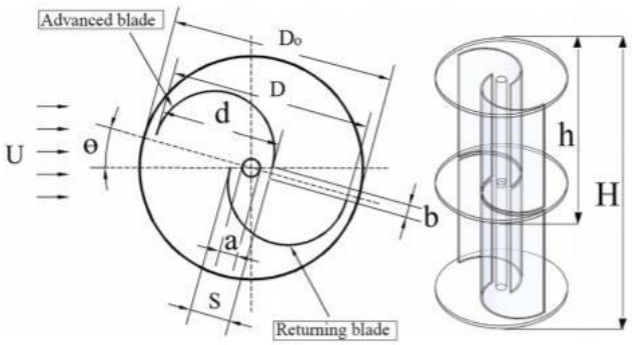

Figure 5: Traditional Savonius Rotor [11].

From the traditional Savonius rotor, many other blade profiles have been developed for different studies by different researchers. Figure 6, shows four different blade profiles which have been used for a study by Roy and Saha. Conventional semi-circular and semi-elliptic classical Savonius profile Figure 6(a,b) is compared in Roy and Saha's work [13]. Whereas Figure 6(c), is developed by Benesh AH in 1996, during that time, it has been claimed to be one of the best small scale wind turbines (SSWT). In the last two decades, much research has been done on the Savonius turbine and currently, Bach type profile is having a great interest among many investigators. In this thesis, the Modified Bach type profile developed by Lundberg, Manousidou, Solhed and Sundberg is selected to study further and optimize its design by considering its efficiency [5].

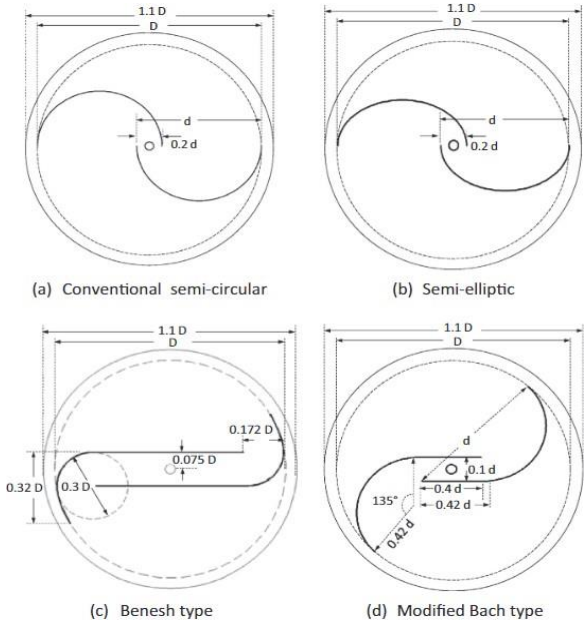

Figure 6: Various blade profiles generated by Roy and Saha [13]

3. Geometry Selection

In this study total three geometries are selected from previous work to be further investigated in this thesis work. In previous work, they investigated the trend of blade arc angles, and it shows that an increase in blade arc angles gives a higher power coefficient. Their results indicate that the 130-degree blade arc angle with an overlap ratio (defined and discussed in section 4.1.1.2) of 0.56 generates maximum power compared to other configurations. For a broad scope, I have selected the three geometries from previous work to investigate the best combination of distance between the blades and the overlap ratio. Figure 7, shows three different geometries with different arc angles. The reason behind selecting three geometries with a difference of 20 degrees was to find the clear trend. Additionally, findings of selected geometries were carried out at TSR 1. The main motivation behind selecting the results at TSR 1 was, turbine gives its maximum efficiency at TSR 1. It can be easily seen in the Cp curve of Savonius turbine figure 3. Ultimately, it will be easy to compare the results with new results.

Table 1: $C_{P,Max}$ and P_{Max} data for different geometries developed by [5].

Blade arc angle	**TSR (λ)**	**$C_{P,Max}$**	**$P_{Max}(W)$**
80°	0.6	0.2165	33.95
90°	0.6	0.2249	35.26
100°	1.0	0.2407	37.75
110°	1.0	0.2396	37.57
120°	0.8	0.2533	39.72
130°	0.9	0.2627	41.19
140°	1.1	0.2532	39.70
150°	1.0	0.2603	40.81

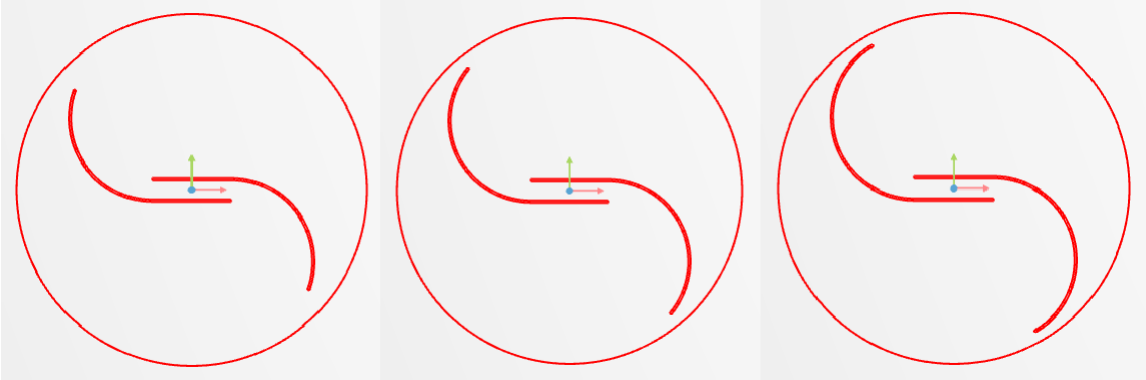

Figure 7: Selected geometries with blade arc angle of 110°, 130° and 150° (left to right)

4. Design and Simulation Methodology

4.1 Software

Two-dimensional design modification in blade profiles is carried out in CAESES software and exported to the ANSYS 2021 R1 software for CFD analysis via CAESES add-ins for the ANSYS workbench. In this section, I will discuss the design modification and simulation methodology briefly.

4.1.1 CAESES

The German company FRIENDSHIP SYSTEMS has developed this Computer Aided Design (CAD) software to support the engineers with simulations and automated design exploration, and shape optimization. CAESES provides the facility to design variables that are essential for design modifications. Design variables are adjustable with their minimum and maximum values, which can be changed from the ANSYS workbench. This plugin gives higher flexibility to simulate different geometries without changing the simulation setup. The aim behind using this platform is to make an automated process of simulation.

4.1.1.1 Design Modification

CAESES software is used to generate the geometry, which can be changed according to desired combinations. The main aim of using this software is to make the simulation process smooth and efficient. Furthermore, when the geometry changes, the simulation needs to be set up from the beginning. There are three design parameters which are varied and studied in this work.

The geometry is created by introducing the points on the plane and using the line and curve tool, all points are connected as per the dimensions given in the previous study. After making the turbine profile, interfacing between the refinement regions and rotating regions are created. For better accuracy, two refinement regions are created around the test object. The reason behind the refinement region is covered in the meshing section.

4.1.1.2 Generated Design Variable Parameters through CAESES

a) Blade arc angle

   The blade arc angle is the angle of the cup from inside to the tip of the blade, and a change in blade arc angle leads to variation in drag forces. Since the Savonius rotor is drag based, it is essential to find the best blade arc angle to make it efficient. Figure 8 shows the illustration of the blade arc angle.

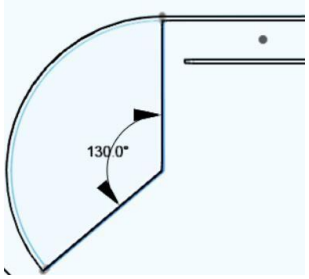

Figure 8 Top view representation of Blade arc angle

b) Distance between blades

The gap between the two blades is simply measured from blade to blade. In this study, distance between blades has been increased and decreased (in the range of 2.5 to 4.5 cm) to find the best combination.

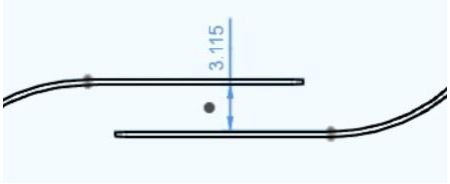

Figure 9 Top view representation of Distance between blades

c) Overlap Ratio

The overlap ratio (OR) is defined as the ratio between the overlap distance and the radius of the blade. For example, for the geometry given in figure 9, Overlap ratio= 6.18/30.57, which is nearly 0.2.

In many studies OR is defined differently according to geometry notation. In this study, OR is investigated after finding the best optimal distance between blades for each blade arc angle case.

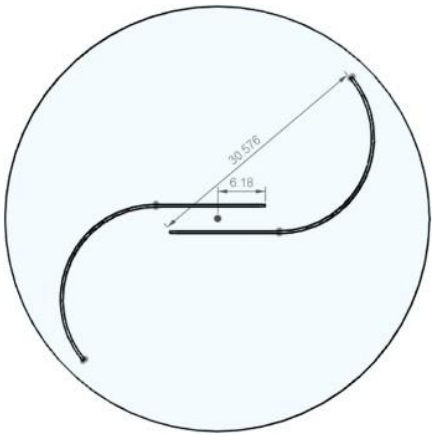

Figure 10: Top view of blade profile with a parameters of Overlap Ratio

4.1.2 Ansys

Ansys is a Multiphysics software widely used for product design, simulations, testing, and operation. Ansys is well known and trusted in industries due to its flexibility and efficiency. Computational analysis is a must to solve the complex flows and systems across the industry. Ansys 2021 R2 has proved its worth in simulating electromechanical, mechanical, fluid dynamics, noise, vibration, and material fatigues.

There are two applications in ANSYS to do CFD simulations, CFX and Fluent. In this thesis, the Ansys Fluent block is used to simulate the fluid flow of the Savonius turbine. Different geometries are investigated in this software. Due to the student license, computational power is limited. A two-dimensional (2D) study is comparatively less time consuming compared to the three dimensional (3D). Due to the time frame and complexity, 2D simulation is used to investigate all the design parameters.

4.1.2.1 Meshing

Meshing is the second step after setting up the geometry and refinement regions. For an efficient solution, correct meshing is essential to get accurate results. Total three different meshing methods are available in Ansys,

I. Quadrilateral Dominant
II. Triangles
III. MultiZone Quad/Tri

According to the meshing guidelines given by Ansys, each of them has its own advantage. A quadrilateral method is highly efficient compared to a triangular one, and third method is a mixture of Quadrilateral and Triangular; it is used for a specific problem that needs compact meshing for investigating the different dependent parameters. The choice of the mesh method depends on the application. The main advantage of unstructured mesh is, It can handle curvature boundaries of arbitrary shape. Quadrilateral Dominant is an efficient method compared to Triangular, but considering the time duration and computational power, the triangular mesh is selected to study the blade profiles. In the mesh setup, a rotating mesh is used internally, and a fixed mesh is used for the refinement regions. Interfaces are created on each refinement region for an easy flow from one refinement to other refinements.

Figure 9 shows the meshing of entire simulation domain. Different rectangular regions represent the each refinement. The reason behind using the refinements is to optimize the simulation time and accuracy of the solution. Brief explanation is covered in simulation setup section.

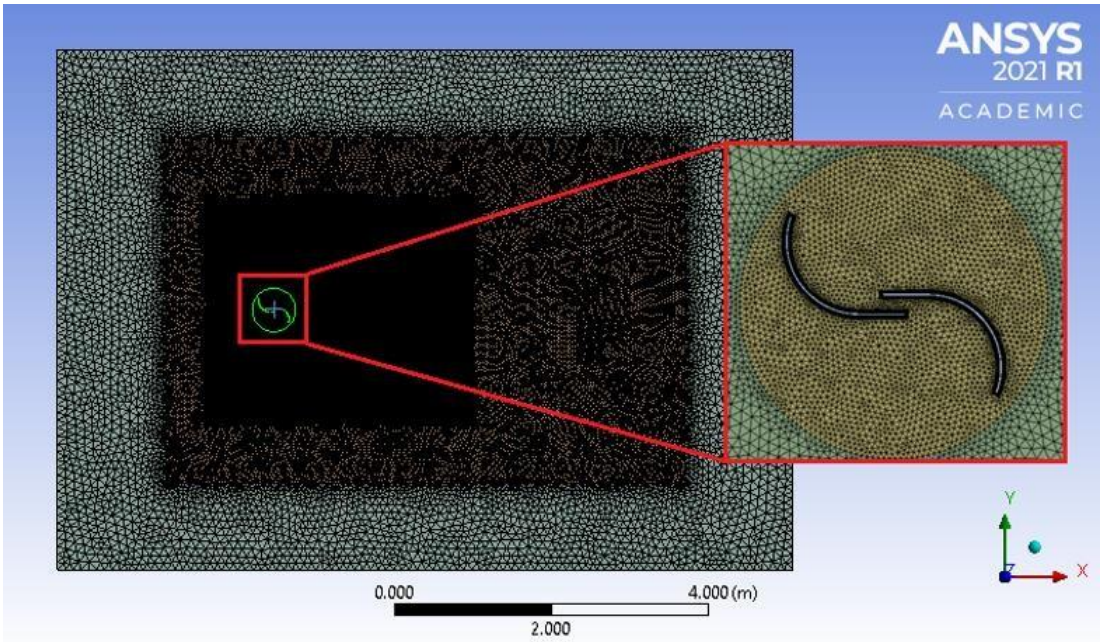

Figure 11: Meshing used for the simulation

4.1.2.2 Blade Inflations

After setting up the meshing method and sizing for all refinements, Blade inflations are added to extract accurate data from the test object (blades). Generally, inflation layers are also part of meshing, and it is used where it requires to capture the wall bounded turbulent flow in the boundary layer. According to the previous study and open-source guides [16], It is suggested to use 10 to 15 layers to get accurate results at the boundary layer of the flow. In this study, 15 inflations are used on both of the blades.

4.1.2.3 Turbulence Model

The selection of turbulence model is important in CFD simulations. Here I have used the k-ω Shear Stress Transport (SST) model to predict the velocity trend at the test point. Most of the studies on Savonius wind turbine have used the same model. k-ω SST model is a two-equation eddy viscosity model. This model is a member of the Reynolds Average Navier Stokes (RANS) family. The main advantage of this model is good behavior in adverse pressure gradients, and it also provides a good prediction of separation of flow [15].

Following equations (4.1) and (4.2) are called Reynolds-averaged Navier-Stokes (RANS) equations [16],

$$\frac{\partial \rho}{\partial t} + \frac{\partial y}{\partial x_i}(\rho u_i) = 0 \quad (4.1)$$

$$\frac{\partial}{\partial t}(\rho u_i) + \frac{\partial}{\partial x_j}(\rho u_i u_j) = -\frac{\partial p}{\partial x_i} + \frac{\partial}{\partial x_j}\left[\mu\left(\frac{\partial u_i}{\partial x_j} + \frac{\partial u_j}{\partial x_i} - \frac{2}{3}\delta_{ij}\frac{\partial u_l}{\partial x_l}\right)\right] + \frac{\partial}{\partial x_j}\left(-\rho\overline{u_i' u_j'}\right) \quad (4.2)$$

RANS equations are the time-averaged equation of fluid flow. In equation (4.2), the left-hand side stands for the change in mean momentum due to turbulence. In order to close the equation (4.2), the Reynolds stresses $-\rho\overline{u_i' u_j'}$ should be modelled.

The mathematical expression of k and ω can be written as following [17],

$$k = \frac{3}{2}(UI^2) \quad (4.3)$$

Equation 4.3 shows the turbulent energy, where U is the mean flow velocity, and I is turbulence intensity. And turbulent intensity can be defined as follows,

$$I = \frac{u'}{U} \quad (4.4)$$

The turbulent specific dissipation rate can be calculated by using the following equation,

$$\omega = C_\mu^{\frac{3}{4}} \frac{k^{\frac{1}{2}}}{l} \quad (4.5)$$

Where, C_μ is the turbulence model constant, with a value of 0.09 and l shows the length of turbulence. By using the k-ω SST model, we are investigating drag forces, lift forces, momentum data and other data which are required to find the efficiency of the turbine. Model configuration and setup steps are discussed briefly in the simulation setup section.

4.1.2.4 Boundary Conditions

In Ansys and other simulation softwares, some of the boundary conditions are usually predefined like in this k -ω turbulence model, velocity, pressure, k and ω are predefined default values. According to the application, user has the flexibility to redefine the boundary conditions as per the requirement. There are two main boundary conditions for the inlet and outlet flow velocity, no-slip and slip boundary conditions. Generally, no-slip boundary condition can be applied in a microfluidic application where solid boundaries and incompressible fluid is used [18].

In this study, boundary condition of domain walls is selected by specifying zero shear. For simulation purpose only boundaries (side walls) are introduced but wind turbines won't be having any side walls. For that reason, fluid flow is assumed as incompressible with the uniform flow of 8 m/s at the inlet. Outlet values of simulation domain is kept as default in Ansys.

4.1.2.5 Wall Y plus

Dimensionless wall distance y^+can be denoted as follows,

$$y^+ = \frac{y u_T}{v} \quad (4.6)$$

In equation (4.6), y is an absolute distance from the wall, v stands for the kinematic viscosity and u_T is friction velocity.

Wall y^+ is the non-dimensional distance between the wall and the first node of the mesh. It is often used in CFD to define the mesh quality for a specific flow. It can be described as a ratio between turbulent and laminar influence in the cell [19]. y^+ has certain limits to validate the turbulence model. According to flow simulation guidelines, for the viscous sublayer the y^+ value should be under 5. An increase in the inflation layer will help in keeping it within the limit. Figure 10 shows the y^+ value near to blades.

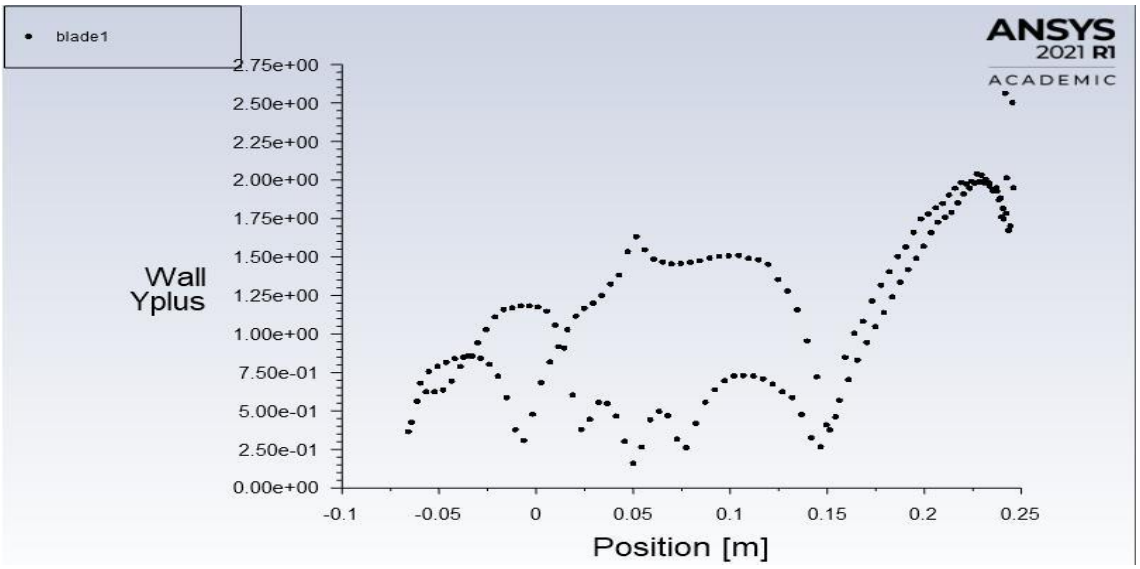

Figure 12: Plot of y^+ plus data values of blade 1

4.1.2.6 CFL criterion

Courant Friedrichs Lewy (CFL) criterion is a stability condition, which is used for the stability of unstable numerical methods. CFL plays an important role in CFD simulations. CFL condition decides the timestep size required for the simulation domain. In Ansys, CFL is addressed as a cell convective courant number. To avoid the numerical oscillations and for accuracy improvement, guidelines indicate that the courant number should be equal to or less than 1 [20]. To get a proper data, flow should not move faster from one mesh cell per time step. Mathematical representation of Courant number is as follows,

$$C = v\frac{\Delta t}{\Delta x} \leq 1 \quad (4.7)$$

Where v is the average linear velocity in the simulation domain, Δt is the maximum time step size, and Δx shows the smallest mesh cell dimension [20].

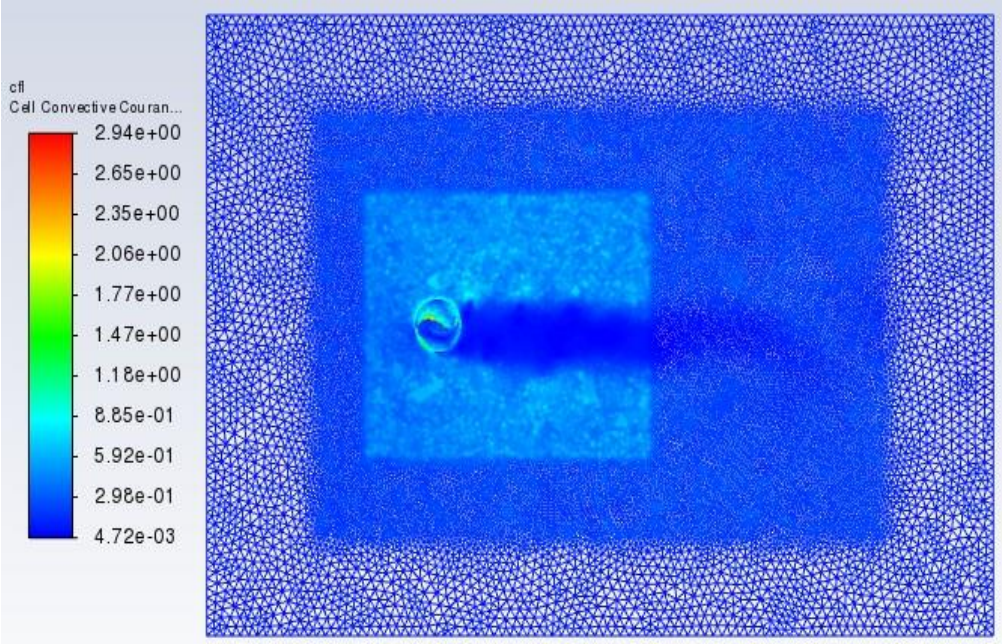

Figure 13: CFL value correction during the ongoing simulation

4.1.2.7 Blockage ratio

The blockage ratio can be defined as the ratio between the frontal area of the turbine to the cross-sectional area of the domain [21]. Generally, blockage ratio is used to account for how much the domain is blocked by the test object (turbine) and how that affects the wind speed travelling through it.

$$Blockage\ Ratio = \frac{Frontal\ area\ of\ the\ turbine}{Cross\ sectional\ area\ of\ domain * 4} \quad (4.8)$$

4.2 Simulation Setup

The simulation setup requires geometry files, and geometry files are generated using CAESES software. The first step is to have a proper CAESES geometry with the design variables. Exported files (.fsc and .sat) should be imported into Ansys workbench in the fluent block by using the CAESES plugin block. Fluent block contains five steps, geometry, meshing, setup, solution, and results. Since we are using imported geometry, CAESES geometry should connect directly to fluent meshing (figure 14).

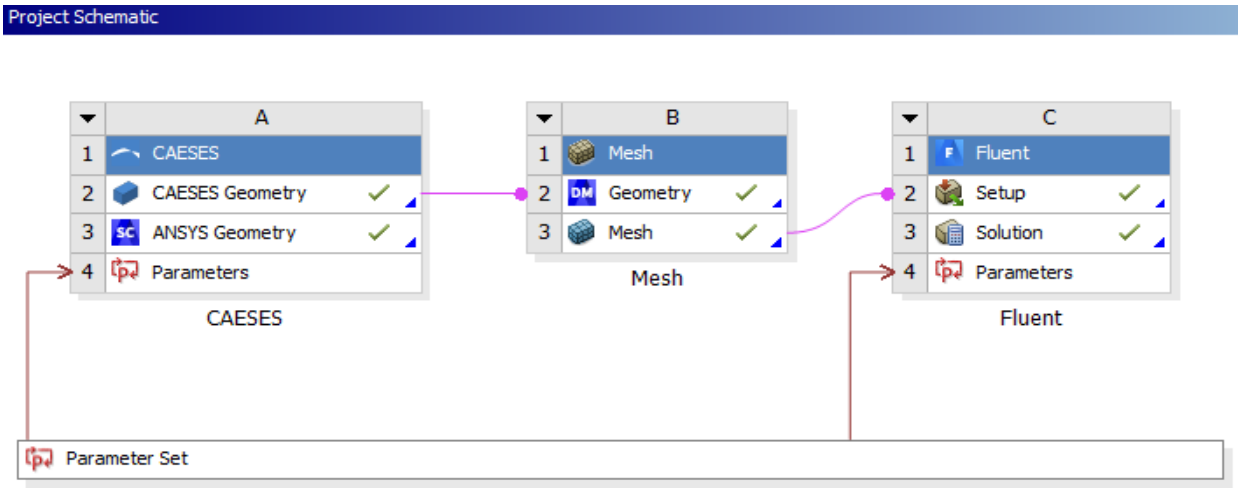

Figure 14: Project Schematic in ANSYS Workbench

This study uses different design geometries, and each geometry has required different meshing. To save time and effort, a scripting method is used for meshing. The general python script defines the name of faces, bodies, interfaces, refinement zones and meshing size. Generated meshes will update by itself in Fluent and then it exports to the Fluent setup. Fluent setup is modified as; Precision setting is selected as Single Precision, which is sufficiently accurate and less time-consuming. Followed by the precision selection, number of processes are selected according to system capacity. After that, a Pressure-Based solver with absolute velocity formation and transient simulation setting is used for more comprehensive results. As discussed previously in 4.1.2.3, the Viscous (SST k-omega) turbulence model is adopted with predefined model constants. After selecting the model, fluid and solid materials have been selected with their predefined density and viscosity.

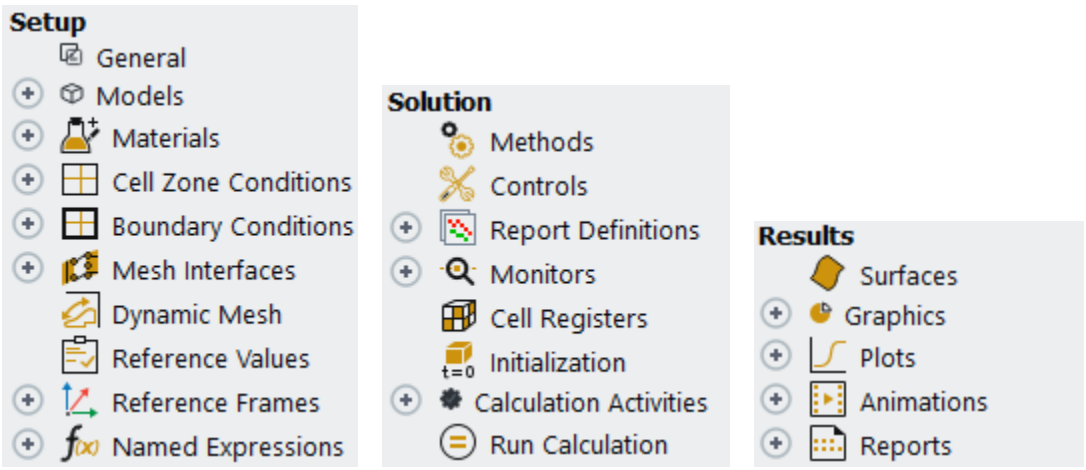

Figure 15: Different phases of Fluent setup

Boundary Conditions are specified as inlet velocity 8 m/s and blade walls are selected as moving at an angular velocity (ω) defined in a parameter set (figure 15), and shear is specified to zero for sidewalls of the domain. In actual, there are no such walls, but in the simulation, we are assuming an equal flow without any shear from the walls. Section 4.1.2.4 gives a brief idea of the boundary conditions. Ansys user guidelines indicated that the coupling algorithm offers an alternative to the pressure-density based segregated algorithm with SIMPLE type pressure-velocity coupling. Settings of spatial discretization, a least square cell-based method is used to solve the gradient. For Pressure, Momentum, Turbulent kinetic energy, and specific dissipation rate are modified as second-order upwind scheme. The benefit of selecting the second-order upwind approach is that it uses two upstream points for computation, and it's more accurate compared to the first order.

Once the method is selected, the report definition is extracted according to the need for data. The first step of defining the report definition is to choose the specific output type. In this study, lift force, drag force, moment data, y^+ and CFL data were extracted. Graphical representation and output file are collected and used for calculating the power coefficient. Before starting any simulation, it is necessary to initialize the flow in the simulation domain. Seeing that, the problem has sliding meshes (meshing of innermost refinement and rotating part, figure 10), the reference frame is selected relative to the cell zone. Additionally, an initial value of velocity in x-direction is set as 8 m/s with a zero gauge value in the Initialization window.

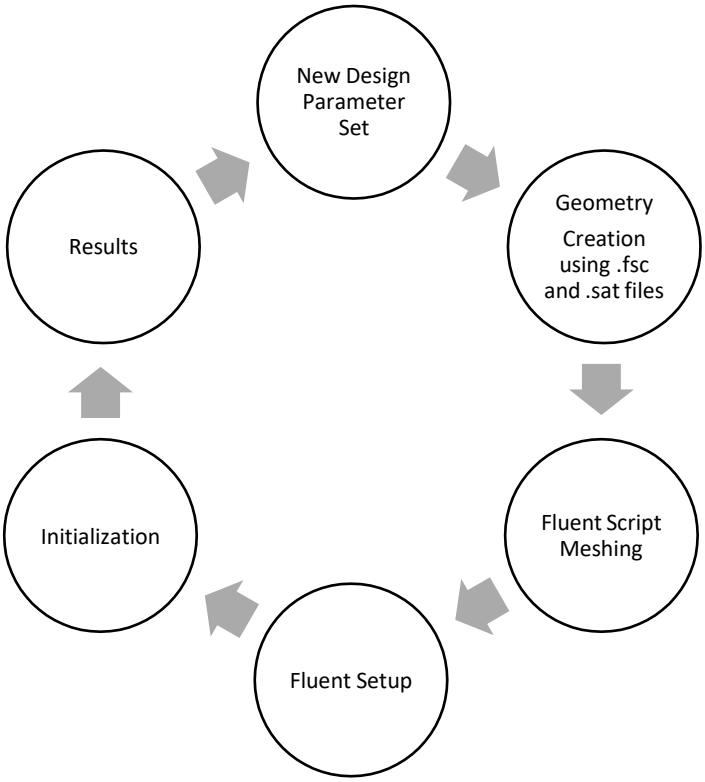

Figure 16: Automated Simulation Cycle

The last step is to set the time steps and time step size. CFL values depend on the time step size, so by doing a couple of simulations, one can assume the time step size. In this study, all the simulations are carried out for 5000 time-steps with 0.0005 sec. time step size. By using higher timesteps and lower time-steps, it was found out that 5000 to 7000 timesteps were giving slightly less performance compared to the previous study, which has used 10000 to 15000 time-steps. In short, more time-steps will give a more accurate average value. So by respecting the time and available computational power, a lower number of time-steps are chosen.

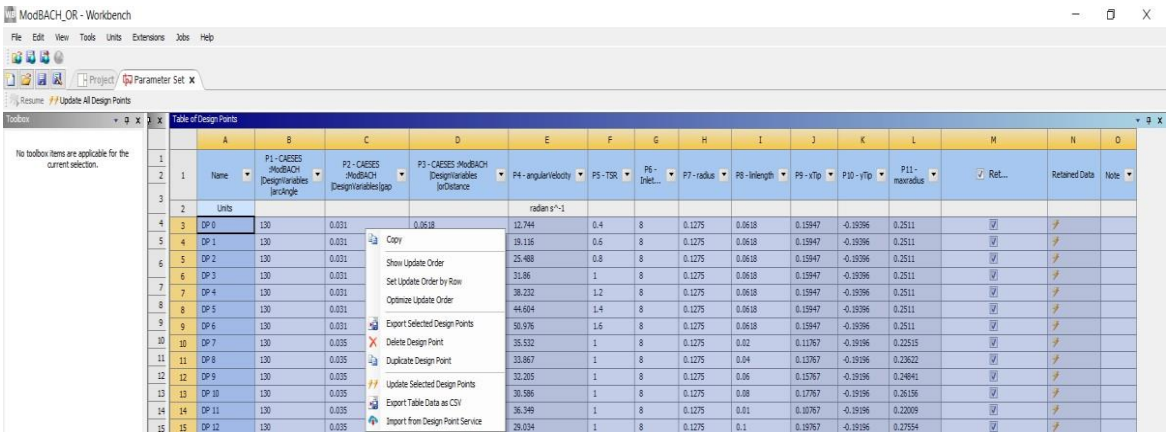

Figure 17: Different geometries in Parameter Set

To start the cyclic automated simulations, different design points are generated as shown in figure 16 and updated those design points by pressing right-click. According to the number of simulations, the system takes time to simulate all design points.

Note: While updating new design points (starting of simulation), CAESES software should be closed; otherwise plugin might create some problems.

4.2.1 Simulation Domain Validation

Simulation data cannot be exact as reality. So validation of simulation setup is required to validate experimental data with previous data. Considering that work is a continuation of previous work by [5], this study uses the same simulation domain as previous work.

The dimension of the simulation domain is shown in figure 16 in terms of turbine diameter (D). The dotted line represents the refinement regions for compact meshing. Table 2 shows the mesh size with different refinements and rotor face. Simulation domain sensitivity findings from [5] suggest that in the 12 diameters wide simulation domain, ModBach has shown the same trend as Blackwell et al. [22].

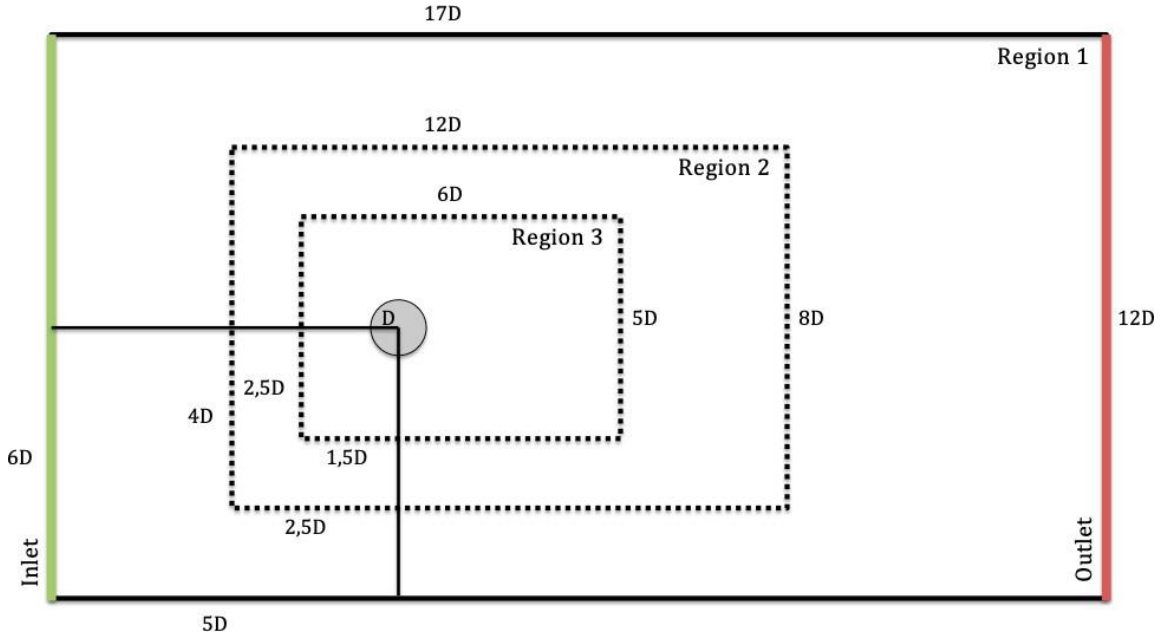

Figure 18: Dimension of simulation domain in terms of turbine diameter [5]

Table 2: Selected meshing size of refinements and rotor face

Refinements	Method	Mesh size (m)
Region 1	Triangular	0.1
Region 2	Triangular	0.04
Region 3	Triangular	0.02
Rotating Region	Triangular	0.01
Turbine blades	Triangular	0.005

5. Results

In this section, we will discuss about the simulation findings and new results, which are compared with previous studies. The effect of rotor performance has been discussed by investigating the distance between blades and overlap ratio modification. The study intends to find the optimized shape of the modified bach Savonius rotor.

5.1 Validation

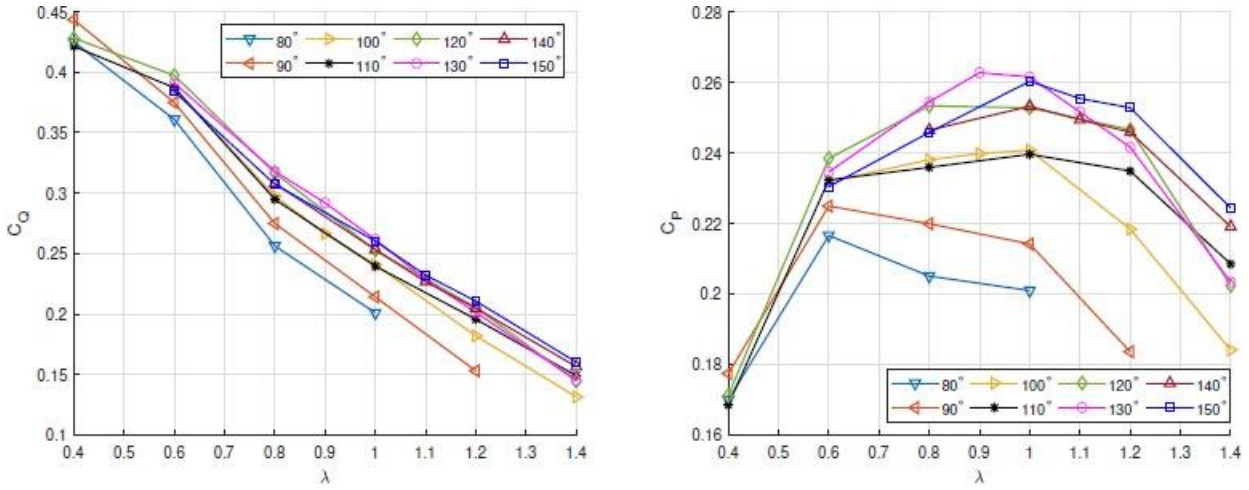

Figure 19: C_q and C_p results for different blade angles[2]

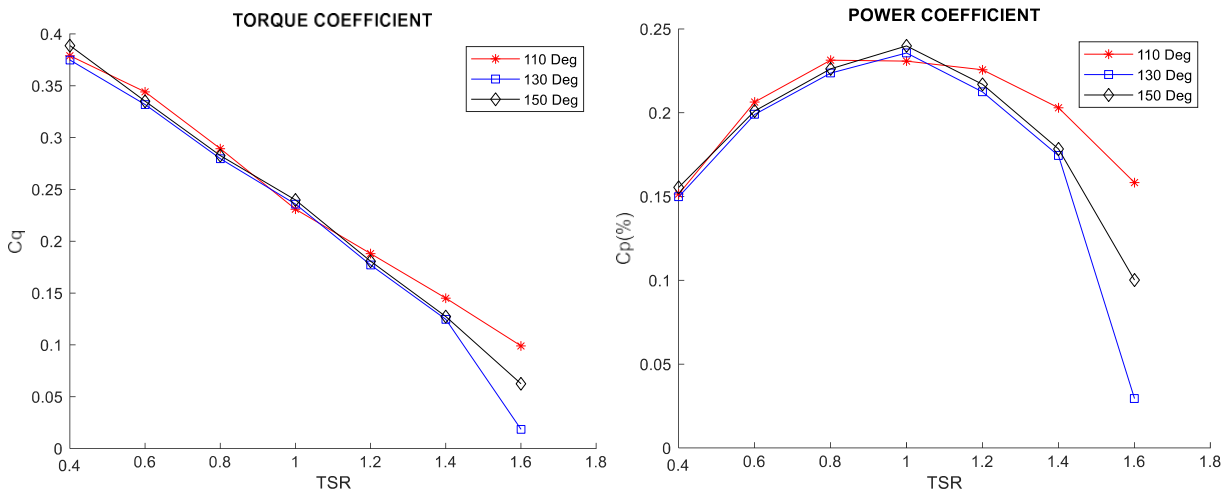

Figure 20: C_q and C_p results of selected blade angles

Figure 17 shows the torque coefficient (C_q) and power coefficient (C_p) of eight blade arc angles. Before starting the study, the simulation setup is validated by performing a range of simulations on the selected geometries (figure 7). For validation of simulation setup, analysis of the number of simulations is taken, and graphs are plotted as seen in figure 18 and the findings were compared

with previous study figure 17. It can be noticed that the power curve of newly created geometries shows almost the same power curve when compared to the previous study. Additionally, most of the designs are giving their best performance at 1 TSR. Hence all the further studies are performed on TSR 1 by varying different parameters, as discussed previously.

5.2 Distance Between Blades

The result of the simulations of the distance between blade profiles is displayed in figure 19. Three blade arc angles (110°, 130° and 150°) are selected for six different combinations of distance from 2.5 cm to 4.5 cm. The reason behind doing the study was to find a proper geometry that gives high efficiency. Out of 18 geometries, a total of three geometries are selected to study further to find a best overlap ratio for each case. In figure 19, for each case, one point is selected where geometry has given the highest efficiency.

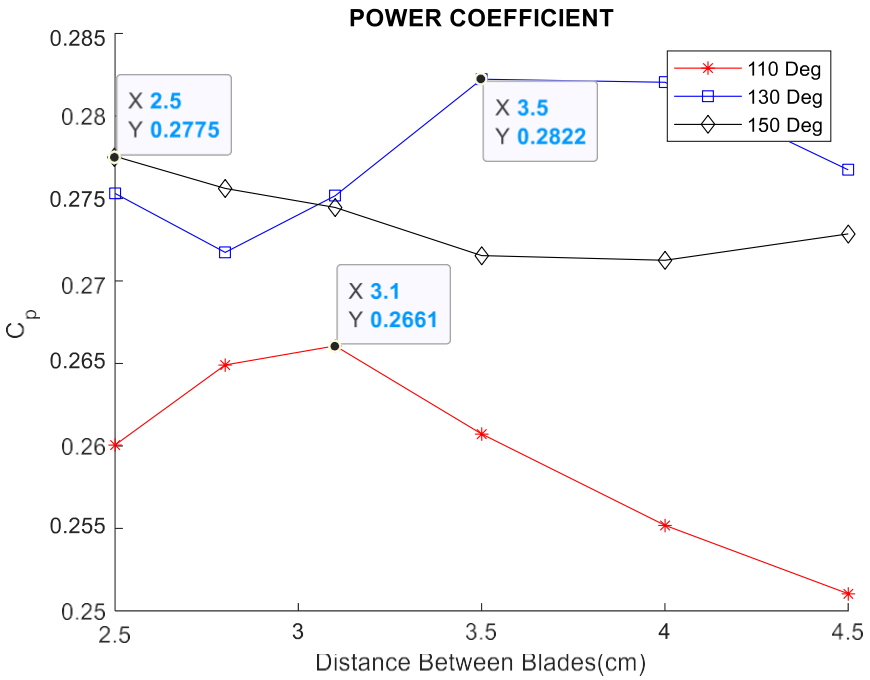

Figure 21: C_p result of 18 geometries by varying the distance between blades(@ TSR=1)

Out of 18 simulations, the one with most efficient geometry was selected for each blade arc angle case, which is highlighted in figure 19. P_{Max} was calculated as seen in the following Table 3. Images of all the selected geometries are attached, followed by Table 3. Newly developed geometries are then compared with the ModBach profiles.

Table 3: Selected best geometries from Distance between blade analysis to investigate OR

Blade arc angle°	Distance Between Blades (cm)	TSR (λ)	$C_{P,Max}$	$P_{Max}(W)$ ($P_{Max} = Q\Omega$)
110	3.1	1	0.26	39.9
130	3.5	1	0.28	44.1
150	2.5	1	0.27	44.9

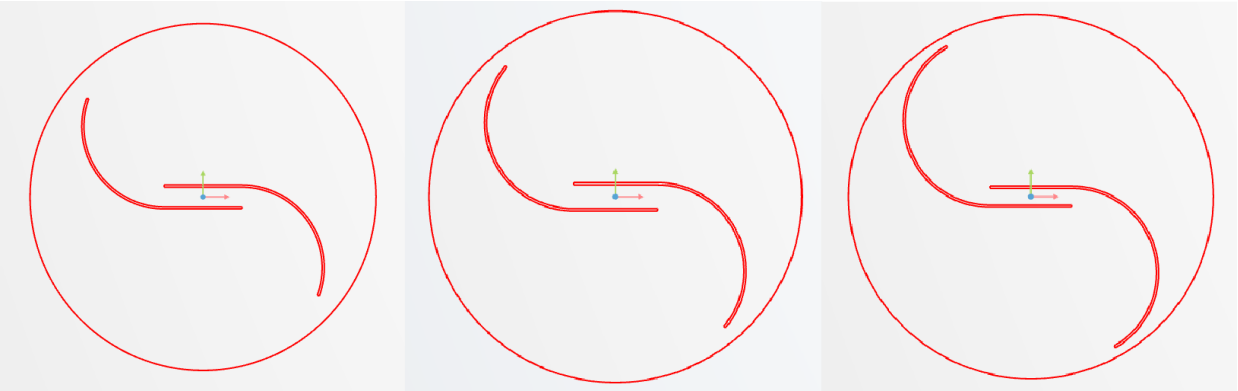

Figure 22: Selected geometries to investigate the overlap ratio. Left to right, first geometry is 110° with 3.1cm, second 130° with 3.5cm, and last 150° with 2.5cm distance between blades

Table 4: Dimensions of Selected Geometries to Investigate the Overlap Ratio

Parameters	110°	130°	150°
Distance between blades	3.1 cm	3.5 cm	2.5 cm
Blade Radius	21 cm	23 cm	24 cm
Diameter of End plate	55 cm	55 cm	55 cm
Blade thickness	0.35 cm	0.35 cm	0.35 cm

5.3 Overlap Ratio

As we discussed in 4.1.1.2 , Overlap ratio is defined as the ratio between overlap distance of blade to the radius of the blades. Mathematically it can be calculated using following equation.

$$Overlap\ Ratio = \frac{Overlap\ Distance}{Radius} \quad (5.1)$$

In the thesis, we are introducing a new term named variable radius. Variable radius is the new radius when we change the overlap distance. A significant increase in overlap distance will also increase the radius of the turbine. Usually, due to a small change in radius, it didn't considered in the previous study of efficiency and power calculations. But, consideration of a change in radius is giving significant rise in the efficiency and generated rated power. In this section, all the calculations are done by considering the individual radius of the turbine blade.

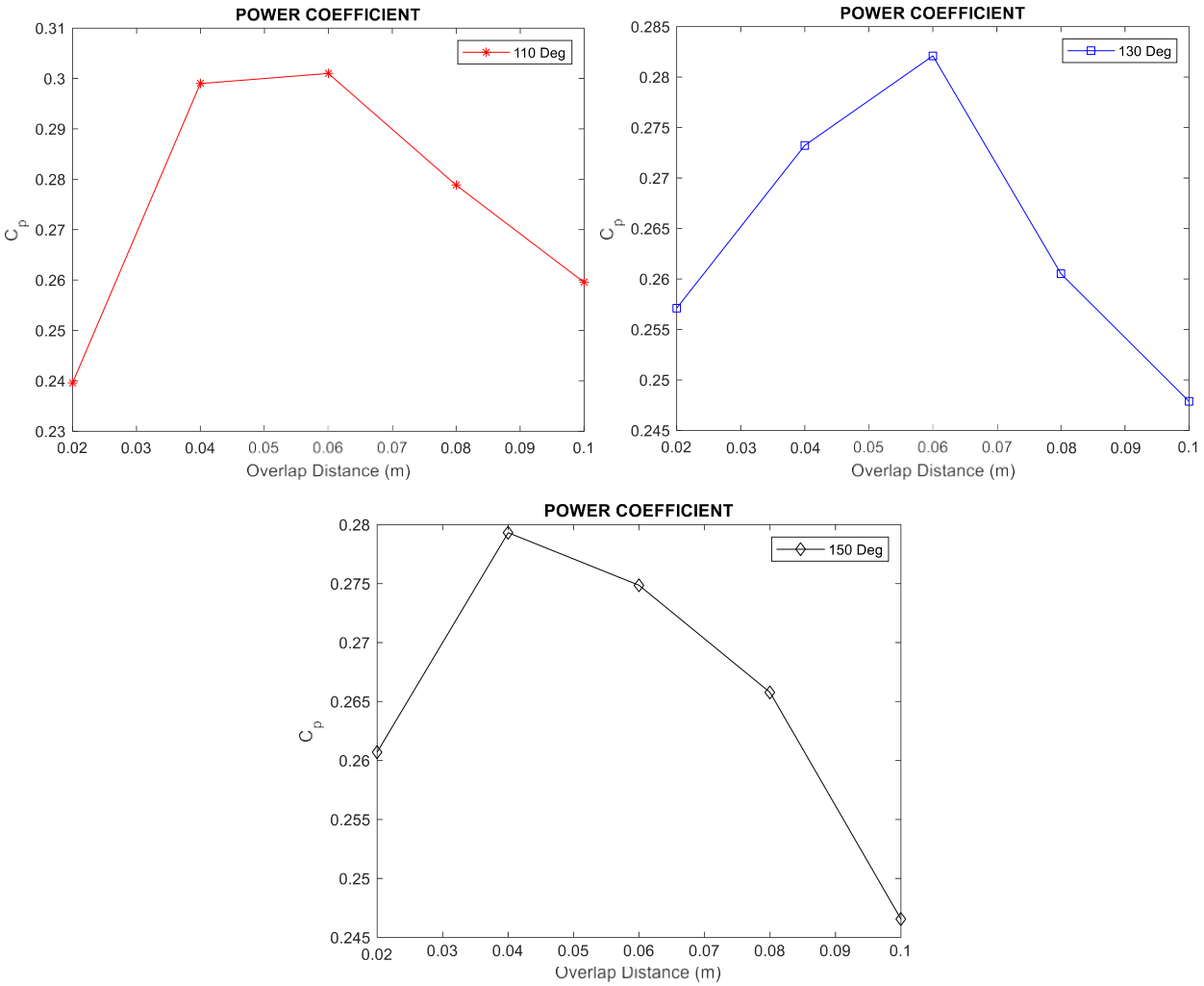

Figure 23: Overlap Distance study of three profiles with different overlap ratios (@TSR=1)

Table 5 shows the result of the overlap ratio study for three selected geometries. Each geometry is investigated with five overlap ratios to find the best combination. After looking into the results, it can be observed that as we increase the overlap ratio power coefficient is also increasing gradually. At a certain point, it again starts to decrease.

Table 5: Study of Overlap Ratio parameter on selected three geometries

Blade arc angle°	**TSR (λ)**	**Overlap Ratio**	**$C_{P,Max}$**	**$P_{Max}(W)$**
110	1	0.09	0.24	31.44
110	1	0.18	0.29	41.83
110	1	0.25	0.30	45.15
110	1	0.32	0.28	44.29
110	1	0.37	0.26	43.85
130	1	0.08	0.25	36.31

130	1	0.17	0.27	40.48
130	1	0.24	0.28	43.95
130	1	0.30	0.26	42.74
130	1	0.36	0.24	42.84
150	1	0.08	0.26	38.86
150	1	0.16	0.28	43.00
150	1	0.23	0.27	44.03
150	1	0.30	0.26	44.14
150	1	0.36	0.25	42.71

An experiment has been done on three blade arc profiles. After investing five different ORs for each case, it's found out that each of them gives the highest efficiency at OR of around 0.24, which is highlighted with green color in Table 5. Other geometries also have shown good performance compared to the most efficient ones.

6. Discussion

The power coefficient curve for three blade arc angles shows the similar curve as studied in the previous work. Hence the simulation setup is validated for the further study for distance between blades and the overlap ratio of blades. Selected geometries were 110°, 130° and 150° blade arc angle profiles.

The results for the C_P curve determine that the peak value for all blade arc angles is approximately at TSR $(\lambda) = 1$. Since the selected geometries are the best ones in the previous study, most of them are showing almost the same C_P values at $\lambda = 1$ with an incoming wind speed of 8 m/s. Outof three geometries, 150° has the highest C_P value (figure 19). In addition to this observation, it can be easily observed that as blade arc decreases, the C_P values also goes down (figure 18). Moreover, another trend is also observed is that 110° arc angle gives higher efficiency at higher tip speed ratios. At the same time, 130° and 150° arc angle profiles decrease in a similar way.

The results for different distances between blades are presented in figure 19. Six designs were created and investigated for each blade arc angle. Distance varied from 2.5 cm to 4.5 cm. In this study, total of 18 geometries were investigated. 110° profile generated C_{Pmax} of 26% with a distance of 3.1 cm between the blades. In addition, 130° profile has given the highest C_{Pmax} of 28% with a distance of 3.5 cm between the blades. Whereas 150° profile gives C_{Pmax} of 27% at 2.5 cm distance. The trend seems to be irregular due to modifications in the blade location. Change in blade location will lead to different drag and lift forces according to turbine geometry. The most efficient ones are selected to study the overlap ratio.

The three listed geometries in Table 3 have the highest efficiencies. Hence those profiles are used to investigate the overlap ratio. For each profile, five overlap ratios are studied to find the best design combination of Modbach. A total of 15 design geometries were created using the parameter set in Ansys fluent, as shown in Figure 15. The findings for the different ORs are presented in figure 21. For each case, different colors were used to compare it with the earlier findings. The first graph in Figure 21 shows the overlap ratio study of the 110° profile with a distance of 3.1 cm between two blades. At 0.25 OR, the turbine is giving the C_{Pmax} of 30% at TSR of 1 and 8 m/s inlet velocity. Additionally, for the other two profiles, 130° with a distance of 3.5 cm is giving C_{Pmax} of 28% with 0.24 OR. Whereas 150° with a distance of 2.5 cm has shown almost the same C_{Pmax} of 27% at 0.23 OR. Apparently, it can be easily noticed that all the profiles (110°, 130° and 150°) are giving the highest C_{Pmax} at 0.24 OR (∓ 0.01).

Since the study's findings are completely based on simulations, they are entirely dependent on the simulation model whether its capable of modelling reality or not. There will always be uncertainties in simulations, and flow cannot be computed perfectly at every place like in reality. 2D simulations are performed for an infinite height of Savonius turbine, so in practice C_p is expected to be lower. More refined mesh and higher computational power could always be an option to get an accurate result. This work has been done on a private PC which has limitations in terms of computational power. Findings can be varied based on the number of time steps and

simulation domain size. By considering the time frame for the work, simulations are performed for 5000 to 7000 time steps with a time step size of 0.0005 sec. This study does not cover the turbulence study, which may affect the manufacturer from imperfections in power output.

7. Conclusion

In this thesis work, an optimal design for the Savonius rotor is developed by using the CFD simulations on a PC. In order to validate the experimental data, simulated values are compared with similar previous work (chapter 5). This study investigates two parameters, overlap ratio and distance between blades. The reason behind investigating these parameters was to find the optimal design by considering the efficiency of the turbine.

In conclusion, 110° profile has given the highest C_{Pmax} of 0.30 by keeping the distance between blades 3.1 cm and OR of 0.25 (Table 5). Comparatively, other profiles have also shown good performance in terms of power. Due to a bounded time frame, a limited number of simulations are performed with a maximum possible simulation power. From the findings, a clear trend is distinguished that different blade arc angles give their highest efficiency at different combinations of the distance between blades. Whereas overlap ratio's trend is quite clear, apparently it can be easily noticed in Table 5, that all the profiles (110°, 130° and 150°) are giving their highest C_{Pmax} at 0.24 OR ($\mp$0.01).

Furthermore, in future there is still a possibility to find more accurate blade profile by gradually varying the blade arc angle with high computational power. In this study only 2D simulations has been performed so in 3D there is chance to find out more detailed vortexes and power calculations. Through this study I believe that for more clear trend between OR and distance between blades, one should investigate the profiles between 130° and 150° arc angles with different combination of overlap ratios by keeping respective distance between blades (Table 3).

References

[1] "GWEC-Global-Wind-Report-2021".

[2] I. Al-Bahadly, "Building a wind turbine for rural home," *Energy for Sustainable Development*, vol. 13, no. 3, pp. 159–165, Sep. 2009, doi: 10.1016/J.ESD.2009.06.005.

[3] J. Chen, Y. Che, and L. Zhao, "Design and research of off-grid wind-solar hybrid power generation systems," *2011 4th International Conference on Power Electronics Systemsand Applications, PESA 2011*, 2011, doi: 10.1109/PESA.2011.5982922.

[4] Johannes and Savonius Sigurd, "Rotor adapted to be driven by wind or flowing water,"Jan. 01, 1929 Accessed: Jul. 04, 2021. [Online]. Available: https://www.freepatentsonline.com/1697574.html

[5] M. Lundberg, A. Manousidou, J. Solhed, and J. Sundberg, "Two-dimensional Study of Blade Profiles for a Savonius Wind Turbine," Bachelor Thesis, Uppsala University, Uppsala, 2020. URL: http://www.teknat.uu.se/student

[6] O. A. Ajayi, "Application of automotive alternators in small wind turbines," Master Thesis, TU Delft, 2012. URL: http://resolver.tudelft.nl/uuid:60a3ca0e-25f0-4892-ae52-300dcb4443ab

[7] F. Castellani, D. Astolfi, M. Peppoloni, F. Natili, D. Buttà, and A. Hirschl, "Experimental vibration analysis of a small scale vertical wind energy system for residential use," *Machines*, vol. 7, no. 2, Jun. 2019, doi: 10.3390/MACHINES7020035.

[8] J. Hylander, G. Sidén, M. D', and A. M. Medaglia, "Vertical Axis Wind Turbines: History, Technology and Applications," Master Thesis, Halmstad University, Halmstad, 2010. URL: http://urn.kb.se/resolve?urn=urn%3Anbn%3Ase%3Ahh%3Adiva-4986

[9] J. F. Manwell, J. G. McGowan, and A. L. Rogers, *Wind Energy Explained: Theory, Design and Application*, Second. John Wiley & Sons Ltd., 2010. Accessed: Oct. 23, 2022. [Online]. Available: http://ee.tlu.edu.vn/Portals/0/2018/NLG/Sach_Tieng_Anh.pdf

[10] M. Ebrahimpour, R. Shafaghat, R. Alamian, and M. S. Shadloo, "Numerical investigationof the Savonius vertical axis wind turbine and evaluation of the effect of the overlap parameter in both horizontal and vertical directions on its performance," *Symmetry (Basel)*, vol. 11, no. 6, 2019, doi: 10.3390/sym11060821.

[11] L. Chen, J. Chen, and Z. Zhang, "Review of the Savonius rotor's blade profile and its performance," *Journal of Renewable and Sustainable Energy*, vol. 10, no. 1, 2018, doi: 10.1063/1.5012024.

[12] Anders. Goude, “Fluid Mechanics of Vertical Axis Turbines : Simulations and Model Development,” PhD dissertation, Uppsala University, Uppsala, 2012.

[13] S. Roy and U. K. Saha, “Wind tunnel experiments of a newly developed two-bladed Savonius-style wind turbine,” *Appl Energy*, vol. 137, pp. 117–125, Jan. 2015, doi: 10.1016/J.APENERGY.2014.10.022.

[14] LEAP CFD Team, “Tips & Tricks: Inflation Layer Meshing in ANSYS | Computational Fluid Dynamics (CFD) Blog – LEAP Australia & New Zealand,” *LEAP Australia*, 2012. https://www.computationalfluiddynamics.com.au/tips-tricks-inflation-layer-meshing-in-ansys/ (accessed Aug. 02, 2021).

[15] “K-Omega and K-Omega SST | Global Settings | SimScale.” https://www.simscale.com/docs/simulation-setup/global-settings/k-omega-sst/ (accessed Aug. 02, 2021).

[16] “ANSYS FLUENT 12.0 Theory Guide - 4.2.2 Reynolds (Ensemble) Averaging.” https://www.afs.enea.it/project/neptunius/docs/fluent/html/th/node46.htm#eq-turb-mom (accessed Sep. 19, 2021).

[17] Florian R. Menter, “Improved two-equation k-omega turbulence models for aerodynamic flows,” 1992. Accessed: Aug. 03, 2021. URL: https://ntrs.nasa.gov/citations/19930013620

[18] B. E. Rapp, “Fluids,” *Microfluidics: Modelling, Mechanics and Mathematics*, pp. 243–263, Jan. 2017, doi: 06 December 2016.

[19] S. M. Salim, M. Ariff, and S. C. Cheah, “Wall y+ approach for dealing with turbulent flows over a wall mounted cube,” *Progress in Computational Fluid Dynamics*, vol. 10, pp. 341–351, 2010.

[20] Z. Boz, F. Erdogdu, and M. Tutar, “Effects of mesh refinement, time step size and numerical scheme on the computational modeling of temperature evolution during natural-convection heating,” *J Food Eng*, vol. 123, pp. 8–16, Feb. 2014, doi: 10.1016/J.JFOODENG.2013.09.008.

[21] Sahini Deepak, “WIND TUNNEL BLOCKAGE CORRECTIONS: A COMPUTATIONAL STUDY,” Master Thesis, Texas Tech University, Texas, 2004. Accessed: Sep. 15, 2021. URL: http://hdl.handle.net/2346/19094

[22] B. F. Blackwell, R. E. Sheldahl, and L.V. Feltz, “Wind Tunnel Performance Data for TWO- and Three-Bucket Savonius Rotors,” *Journal of Energy*, vol. 2, no. 1977, pp. 160–164, 1977, doi: 10.2514/3.47966.

8. Appendix

8.1 Studied parameters in this study

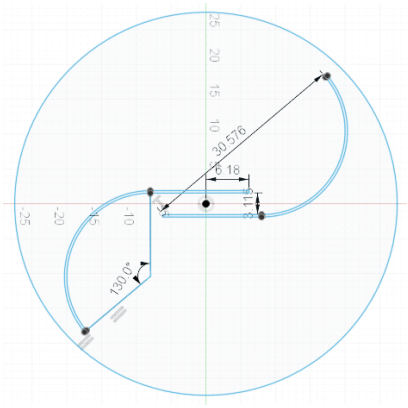

Figure 24 Top view visual representation of Savonius rotor profile

8.2 Dimensions of important geometries from Study 1&2

From Study 1 total 3 geometries were selected which has good combination of distance between blades. The geometry dimensions are listed in following table.

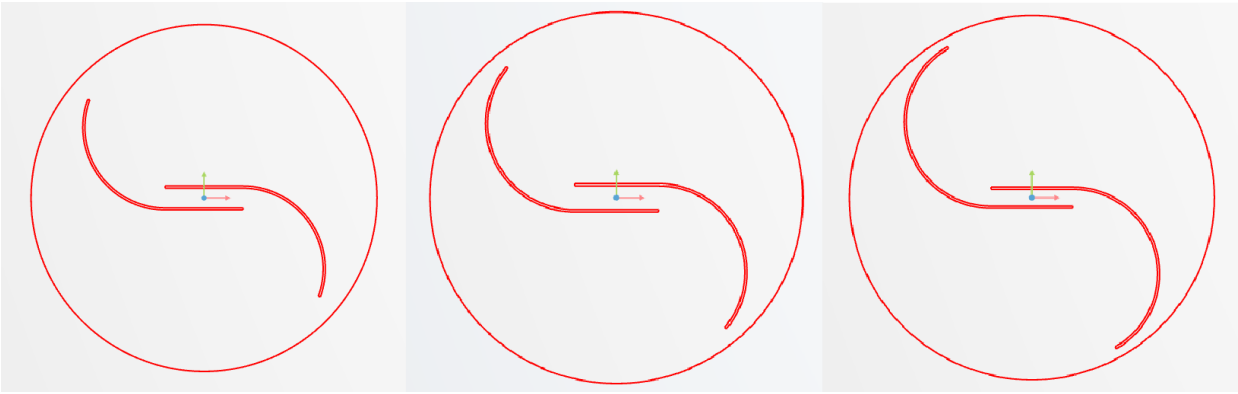

Figure 25 Selected blade profiles 110°,130°,150° (left to right)

Parameters	110°	130°	150°
Distance between blades	3.1 cm	3.5 cm	2.5 cm
Blade Radius	21 cm	23 cm	24 cm
Diameter of End plate	55 cm	55 cm	55 cm
Blade thickness	0.35 cm	0.35 cm	0.35 cm

In Study 2 above mentioned 3 geometries were investigated to find out the best overlap ratio. The dimensions of best combination for each blade arc angle are listed in following table.

Parameters	110°	130°	150°
Overlap Distance	6 cm	6 cm	4 cm
Overlap Ratio	0.25	0.24	0.23
Blade Radius	24 cm	25 cm	25 cm
Diameter of End plate	55 cm	55 cm	55 cm
Blade thickness	0.35 cm	0.35 cm	0.35 cm

8.3 Selection of Vicous Model costants which are used in the simulations

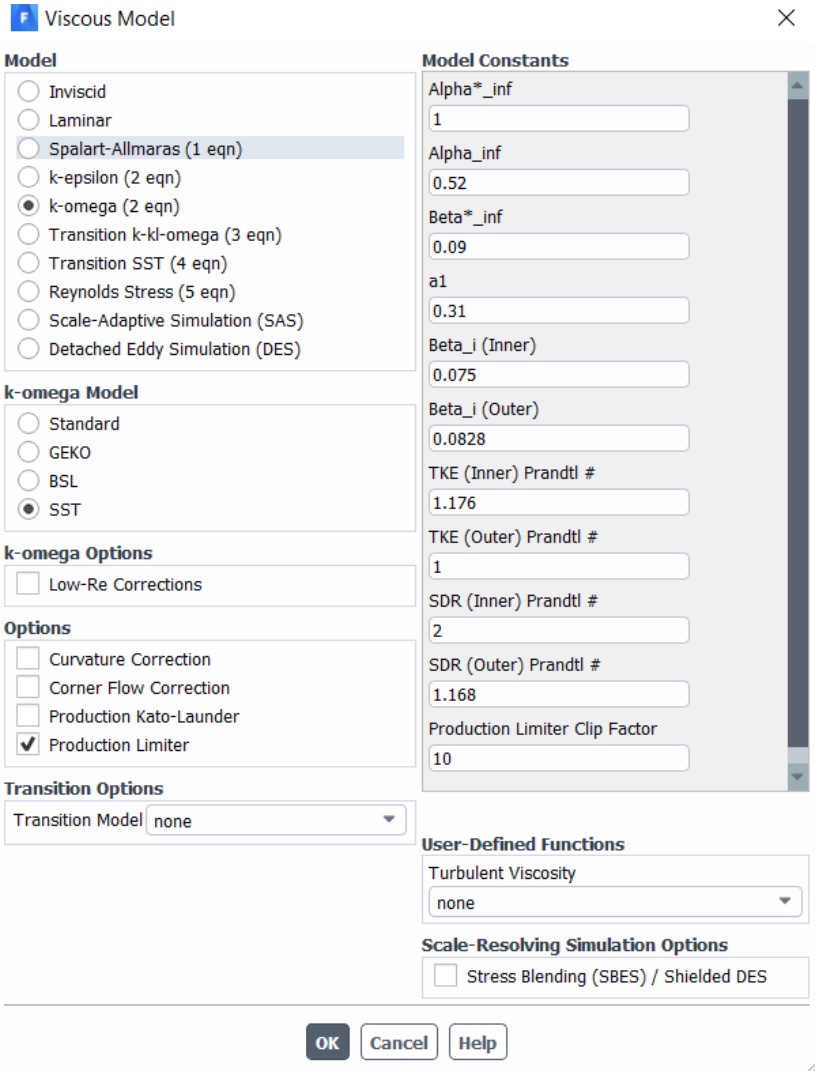

Figure 26 Selection of Viscous Model constants